JCTC Journal of Chemical Theory and Computation

Robust Periodic Hartree−Fock Exchange for Large-Scale Simulations Using Gaussian Basis Sets

Manuel Guidon, Jürg Hutter, and Joost VandeVondele*

Physical Chemistry Institute, University of Zurich, Winterthurerstrasse 190, CH-8057 Zurich, Switzerland

Received September 17, 2009

Abstract: Hartree−Fock exchange with a truncated Coulomb operator has recently been discussed in the context of periodic plane-waves calculations [Spencer, J.; Alavi, A. *Phys. Rev. B: Solid State*, **2008**, *77*, 193110]. In this work, this approach is extended to Gaussian basis sets, leading to a stable and accurate procedure for evaluating Hartree−Fock exchange at the Γ-point. Furthermore, it has been found that standard hybrid functionals can be transformed into short-range functionals without loss of accuracy. The well-defined short-range nature of the truncated exchange operator can naturally be exploited in integral screening procedures and makes this approach interesting for both condensed phase and gas phase systems. The presented Hartree−Fock implementation is massively parallel and scales up to ten thousands of cores. This makes it feasible to perform highly accurate calculations on systems containing thousands of atoms or ten thousands of basis functions. The applicability of this scheme is demonstrated by calculating the cohesive energy of a LiH crystal close to the Hartree−Fock basis set limit and by performing an electronic structure calculation of a complete protein (rubredoxin) in solution with a large and flexible basis set.

1. Introduction

The construction of reliable models for the exchange and correlation energy of electrons is an active research field within the density functional theory (DFT) community. For nearly 50 years, new ideas and approximations have been proposed that increase the accuracy and are improvements compared to the local density approximation[1,2] (LDA). Nowadays, most new functionals go beyond the semilocal generalized gradient approximations[3−5] (GGAs) by incorporating a certain amount of Hartree−Fock exchange (HFX) or similar nonlocal functionals.[6−11,12] Generally, these hybrid functionals are more accurate than their local counterparts. Whereas the use of these hybrid functionals is well established in the quantum chemistry community for the study of molecules, condensed phase systems, such as liquids or solids, are usually treated at a GGA level. Not only is the cost of computing exchange interactions in large condensed phase systems significant, the technical difficulty of obtaining results that are accurate and properly converged cannot be underestimated in calculations employing periodic boundary conditions (PBC). In this work, a robust and accurate scheme, suitable for large condensed phase systems is presented.

In recent work, ref 13, we have presented a linear scaling implementation of HFX that makes it feasible to perform large-scale molecular dynamics simulations with hybrid functionals in PBC. The focus on large systems has guided several design decisions for the implementation. Atom-centered Gaussian basis functions are employed, which makes a linear scaling implementation, based on a screening with the density matrix elements, relatively straightforward.[14−16] Additionally, large systems can be described without **k**-point sampling, and the approach is, thus, Γ-point only. All algorithms are massively parallel and focus on in-core operation to allow for thousands of MD steps in a reasonable time. Our initial implementation of periodic HFX at the Γ-point has been based on an approach by Challacombe and co-workers.[17] In this scheme, the minimum image convention (MIC) is applied at the level of primitives while computing the four center integrals. This is efficient and has been shown to accurately converge to reference results as

* Corresponding author. E-mail: vondele@pci.uzh.ch.

10.1021/ct900494g CCC: $40.75
Published on Web 10/20/2009

the system size is increased.[17] However, it has been observed that this approximation is generally unstable if extended or flexible Gaussian basis sets are used. The instability is the result of a spurious minimum in the energy functional, yielding an unphysical wave function with a total energy that can be several Hartrees beyond the physical solution. This is similar to the behavior observed in traditional HFX calculations that employ a too loose screening threshold. As will be discussed in more detail below, in the MIC, there is no screening parameter which can be adjusted to guarantee stability. The new approach presented here does not employ the MIC, only requires the Γ-point, and is stable with large and flexible basis sets. The use of the truncated Coulomb (TC) operator[18] is a key ingredient. All algorithms and methods presented are implemented within the framework of the CP2K/Quickstep[19,20] program, a freely avaliable molecular simulation package.

2. The Truncated Coulomb Operator for Calculations at the Γ-point Using Gaussian Basis Sets

2.1. Periodic Hartree−Fock calculations. For finite systems such as molecules, which employ open boundary conditions, the HFX energy is computed from its definition:

$$E_x^{\text{open}} = -\frac{1}{2}\sum_{i,j}\int\int \psi_i(r_1)\psi_j(r_1)g(|r_1 - r_2|) \times \psi_i(r_2)\psi_j(r_2)d^3r_1 d^3r_2 \quad (1)$$

The potential $g(|r_1 - r_2|) = 1/(|r_1 - r_2|) = 1/r_{12}$ in conventional HFX calculations but is commonly replaced by other operators, such as $\text{erfc}(\omega r_{12})/r_{12}$, $\exp(-\omega^2 r^2)$ or $\exp(-\omega r)/r$ in modern electronic structure theory.[7,8,21,22] Computing this energy poses no special problems. In the condensed phase, the HFX energy must take the periodic nature of the system into account, and an integration over **k**-vectors, which reflects the translational invariance and the infinite nature of the system, is formally required. In practice, a finite mesh of **k**-points is employed, which usually becomes less dense as the unit cell increases in size. The HFX energy in periodic systems is, thus, defined as

$$E_x^{\text{PBC}} = -\frac{1}{2N_{\text{k}}}\sum_{i,j}\sum_{\mathbf{k},\mathbf{k}'}\int\int \psi_i^{\mathbf{k}}(r_1)\psi_j^{\mathbf{k}'}(r_1)g(|r_1 - r_2|) \times \psi_i^{\mathbf{k}}(r_2)\psi_j^{\mathbf{k}'}(r_2)d^3r_1 d^3r_2 \quad (2)$$

Where N_{k} is the number of **k**-points within the Brillouin zone, and the integrals are over all space. The wave functions are assumed to be normalized over the crystal volume $N_{\text{k}}V$, where V is the volume of the unit cell. This expression, however, is troublesome to compute. The reason for this is the integratable singularity at $\mathbf{k} = \mathbf{k}'$, which is related to the conditionally convergent nature of the integral for that choice of **k**-vectors. Several schemes have been developed to obtain good convergence with respect to the **k**-point sum.[23−27] Of particular interest here is the method by Spencer and Alavi.[18] This method is based on the observation that the TC operator:

$$g_{\text{TC}}(r_{12}) = \begin{cases} \dfrac{1}{r_{12}}, & r_{12} \le R_c \\ 0, & r_{12} > R_c \end{cases} \quad (3)$$

yields an expression for the HFX energy that does not exhibit a singularity at $\mathbf{k} = \mathbf{k}'$, that converges to the exact expression as R_c goes to infinity, and that becomes increasingly easy to converge in **k**-space as R_c becomes smaller. It is intuitive that, contrary to the Hartree energy, the exchange energy converges rapidly with R_c for the TC operator. Since the convergence of the exchange energy is related to the decay of the density matrix, it will be most rapid for systems with a large gap. However, this also means that the minimum R_c, which yields a properly converged exchange energy, is a system-dependent property. As illustrated in Section 3, the exchange energy computed with g_{TC}, in open systems or with full **k**-point convergence, decreases monotonically to its limiting value for increasing R_c. Clearly, one can define truncated versions of other commonly employed operators. In ref 18, it is demonstrated that it is reasonable to take the number of **k**-points as

$$N_{\text{k}} \approx \frac{4\pi}{3}R_c^3\frac{1}{V} \quad (4)$$

(see that work for an in-depth discussion). Once R_c is fixed, eq 4 shows that the Γ-point alone will be sufficient for large systems, since large systems imply a large V. For a cubic unit cell with edges of length L, eq 4 suggests that having $R_c < 0.62L$ is sufficient for Γ-point only sampling. If needed, sufficiently large systems can always be obtained by replicating the unit cell in all directions. The Γ-point expression for the exchange energy is given by

$$E_x^{\Gamma} = -\frac{1}{2}\sum_{i,j}\int\int \psi_i^{\mathbf{0}}(r_1)\psi_j^{\mathbf{0}}(r_1)g_{\text{TC}}(|r_1 - r_2|) \times \psi_i^{\mathbf{0}}(r_2)\psi_j^{\mathbf{0}}(r_2)d^3r_1 d^3r_2 \quad (5)$$

This expression for E_x^{Γ} looks similar to the one for E_x^{open} (eq 1). However, E_x^{Γ} will diverge for $R_c \to \infty$. It has to be emphasized that only for a finite range of R_c, i.e. sufficiently small to allow for Γ-point only sampling of the integral, E_x^{Γ}, as defined by eq 5, will be a meaningful approximation to the full **k**-space integrated HFX energy. A hand-waving argument for the fact that the Γ-point only expression implies a limit on R_c can also be made as follows: for well localized electrons (i.e., if the maximally localized Wannier functions fit the unit cell), the exchange energy between electrons in different unit cells of the system is small. However, eq 5 would nevertheless predict a large contribution to the exchange energy for an electron and its 'periodic image' if R_c is large enough. This spurious 'self-exchange' with the image electron should not be present, and R_c needs, thus, to be chosen accordingly. Based on this reasoning, a somewhat more conservative rule than eq 4 for determining the maximum R_c can be proposed: R_c should be smaller than or equal to the radius of the largest sphere that fits the unit cell. This guarantees, for localized electrons, that no interactions with image electrons are possible. For cubic unit cells this yields $R_c \le L/2$, similar to eq 4, while for orthorhombic

or strongly distorted triclinic unit cells, this estimate can be significantly different from eq 4.

The expression for the Hartree−Fock energy at the Γ-point (eq 5) can be computed per unit cell and in an atom-centered basis set as

$$E_x^{\Gamma} = -\frac{1}{2} \sum_{\lambda\sigma\mu\nu} P^{\mu\sigma} P^{\nu\lambda} \sum_{\mathbf{abc}} (\mu\nu^{\mathbf{a}}|\lambda^{\mathbf{b}}\sigma^{\mathbf{b+c}})_{g_{\mathrm{TC}}} \quad (6)$$

with **a**, **b**, and **c** denoting translations of the unit cell. This exact result can be obtained easily by introducing in eq 5 the expression of the periodic wave function in an atomic orbital basis:

$$\psi_i(r) = \sum_{\mu\mathbf{a}} C^{\mu i} \varphi_{\mu}^{\mathbf{a}}(r) \quad (7)$$

Here, $C^{\mu i}$ are the wave function coefficients, which are complex in the general case but can be taken real at the Γ-point. $\phi_{\mu}^{\mathbf{a}}(r)$ is the atom-centered basis sets, translated by a multiple of the unit cell given by **a**. The density matrix elements $P^{\mu\nu}$ are obtained from $\sum_i C^{\mu i} C^{\nu i}$. The two-electron four center integrals are defined as

$$(\mu\nu^{\mathbf{a}}|\lambda^{\mathbf{b}}\sigma^{\mathbf{b+c}})_{g_{\mathrm{TC}}} = \int\int \mu(\mathbf{r}_1)\nu^{\mathbf{a}}(\mathbf{r}_1) g_{\mathrm{TC}}(r_{12}) \lambda^{\mathbf{b}}(\mathbf{r}_2)\sigma^{\mathbf{b+c}}(\mathbf{r}_2)\mathrm{d}\mathbf{r}_1\mathrm{d}\mathbf{r}_2 \quad (8)$$

These integrals can be obtained analytically for the TC operator, and their numerical treatment will be discussed in detail in Section 2.3. The triple sum over the lattice vectors in eq 6 converges quickly in **a** and **c** because the overlap of the corresponding Gaussian basis functions decays quickly with distance, while the sum over **b** is finite by virtue of the short-range nature of the truncated Coulomb operator. In eq 6, all terms that are larger than a given screening threshold $\varepsilon_{\mathrm{screening}}$ should be retained. As discussed in more detail in section 4.3, screening based on the traditional Schwarz-inequality combined with a simple distance criterium based on the centers of the product densities $\mu\nu^{\mathbf{a}}$ and $\lambda^{\mathbf{b}}\sigma^{\mathbf{b+c}}$ can be used to eliminate negligible terms.

At this point, some differences and similarities between the approach summarized by eq 6, and the MIC, proposed in ref 17 shall be discussed. First, there is the difference in operator $g(r)$, which is the conventional $1/r$ in the MIC and TC operator (eq 3) here. Second, in the MIC, one retains only one term from the sum over **b**, i.e., that particular index **b′**, which guarantees that the distance between the centers of the product densities $\mu\nu^{\mathbf{a}}$ and $\lambda^{\mathbf{b}'}\sigma^{\mathbf{b}'+\mathbf{c}}$ is as small as possible. This is usually the dominant contribution to the sum but generally ignores terms larger than a given $\varepsilon_{\mathrm{screening}}$. With increasing basis set size and quality, this leads to a spurious minimum in the MIC HFX energy functional. This instability is illustrated in Table 1 and analyzed in some more detail in the Section 4.2. Note that for potentials with shorter range, such as $\mathrm{erfc}(\omega r)/r$, the instability is less pronounced. The new method based on the TC operator and the full sum is stable for all basis sets employed, as shown in Table 2. The total energy converges rapidly with R_c reaching, for this simple system, a plateau at $R_c \approx 4$ Å. As expected, for R_c larger than the value suggested by eq 4, 7.7 Å for this system,

Table 1. PBC Hartree−Fock Total Energies [Hartree] Computed with the Minimum Image Convention for Two Operators[a,b]

	total energy [au]	
basis set	$1/r$	$\mathrm{erfc}(\omega r)/r$
SZV	−33.531805	−32.552246
DZVP	−33.781652	−32.801068
TZVP	−33.798435	−32.817981
TZV2P	−83.287255	−33.827285
QZV2P	−219.806121	−41.438744

[a] The conventional $1/r$ Coulomb potential and the short-range potential $\mathrm{erfc}(\omega r)/r$ with $\omega = 0.11$. [b] The system consists of two water molecules, described with pseudo potentials, in a cubic unit cell with $L = 12.42$ Å and with a geometry that appears sensitive to the instability. It can be observed that the total energy converges to an unphysical result as soon as the basis set quality reaches TZV2P.

Γ-point sampling is not sufficient anymore, and the integral diverges. Also the more conservative choice ($R_c = L/2$ for cubic cells) gives good results. Comparing Tables 1 and 2, it can be seen that the MIC results equal the results of the truncated method with $R_c = L/2$ to micro-Hartree accuracy, in the case where the MIC procedure is stable, i.e. the SZV, DZVP, and TZVP basis sets. Even though the instability of the MIC procedure is fundamental, this approach is, by construction, able to eliminate the spurious self-exchange with image electrons, even if the conventional Coulomb operator is used. Further validation and testing of the truncated Coulomb potential method based on eq 6 is presented in Section 3.

2.2. A long-range correction to the truncated Coulomb operator. In the limit $R_c \rightarrow \infty$, the truncated and full Coulomb potential become identical. In the context of hybrid density functionals, the question arises whether the missing long-range exchange at finite R_c can be corrected by the long-range part of a local density functional. In a similar fashion, this has been done for the HSE06[7,8] hybrid functional that uses the short-range $\mathrm{erfc}(\omega r)/r$ potential. The basic concept behind this range separation relies on the fact that the exchange energy can be written in terms of the spherically averaged exchange hole $\rho_{\mathrm{xc}}^{\mathrm{SA}}(\mathbf{r}, s)$:

$$E_{\mathrm{x}}^{\mathrm{DFT}}[\rho] = \frac{1}{2}\int \rho(\mathbf{r})\mathrm{d}\mathbf{r} \int_0^{\infty} 4\pi u \rho_{\mathrm{xc}}^{\mathrm{SA}}(\mathbf{r}, u)\mathrm{d}u \quad (9)$$

where u denotes the electron−electron interaction distance. The long-range part for a system that interacts via a truncated Coulomb potential is then simply given by

$$E_{\mathrm{x}}^{\mathrm{DFT,LRC}}[\rho] = \frac{1}{2}\int \rho(\mathbf{r})\mathrm{d}\mathbf{r} \int_{R_c}^{\infty} 4\pi u \rho_{\mathrm{x}}^{\mathrm{SA}}(\mathbf{r}, u)\mathrm{d}u \quad (10)$$

Within this range-separation ansatz, the exchange energy can be written as

$$E_{\mathrm{x}} = E_x^{\mathrm{HF,TC}} + E_{\mathrm{x}}^{\mathrm{DFT,LRC}} \quad (11)$$

For convenience, a model with an analytical expression of the spherically averaged exchange hole has been chosen. Similar to the range-separated hybrid functional of Heyd et al., the starting point for the long-range correction is the exchange hole formulation of the PBE functional by Ernzerhof and Perdew.[28]

Table 2. PBC Hartree−Fock Total Energies [Hartree] with the Scheme for the Truncated Coulomb Operator For Various Choices of R_c [Å][a]

cutoff radius, R_c	SZV	DZVP	TZVP	TZV2P	QZV2P
0.5	−30.074404	−30.273802	−30.298149	−30.309740	−30.330732
1.0	−32.693538	−33.024934	−33.052548	−33.061415	−33.064684
2.0	−33.459119	−33.722827	−33.738480	−33.747451	−33.750486
3.0	−33.527563	−33.778845	−33.794977	−33.803751	−33.807027
4.0	−33.531707	−33.781608	−33.798342	−33.807131	−33.810757
5.0	−33.531804	−33.781651	−33.798433	−33.807222	−33.810894
6.0	**−33.531805**	**−33.781652**	**−33.798435**	**−33.807224**	**−33.810898**
7.0	−33.531805	−33.781652	−33.798435	−33.807224	−33.810898
8.0	−33.531806	−33.781652	−33.798436	−33.807225	−33.810900
10.0	−33.533982	−33.783206	−33.800223	−33.809006	−33.812843
12.0	−33.912427	−34.152952	−34.170470	−34.179272	−34.183189
16.0	−33.533982	−35.851041	−35.869063	−35.877848	−35.882304

[a] The system is the same as the one described in Table 1, but the results are stable, independent of the basis set. For large values of R_c, the Γ-point sampling of the exchange energy is not sufficient. As discussed in the text, the choice of $R_c \approx L/2 \approx 6.0$ Å (shown in bold) guarantees that no spurious self-exchange parts enter the Γ-point calculation.

The PBE exchange energy is defined via an integral over the exchange energy density $\varepsilon_x^{\mathrm{PBE}}$:

$$E_x^{\mathrm{PBE}} = \int \rho(\mathbf{r})\varepsilon_x^{\mathrm{PBE}}(\rho, \nabla\rho)\mathrm{d}\mathbf{r} \tag{12}$$

$\varepsilon_x^{\mathrm{PBE}}$ is a function of the electron density $\rho(\mathbf{r})$ and its gradient $\nabla\rho(\mathbf{r})$ and is defined as the product of the LDA exchange energy density and the enhancement factor F_x^{PBE} that additionally depends on the gradient of the electronic density:

$$\varepsilon_x^{\mathrm{PBE}}(\rho, \nabla\rho) = \varepsilon_x^{\mathrm{LDA}}(\rho) \times F_x^{\mathrm{PBE}}(\rho, \nabla\rho) \tag{13}$$

The PBE exchange hole model J_x^{PBE} enters into the definition of the enhancement factor, defining the latter to be an integral of the following kind:

$$F_x^{\mathrm{PBE}}(s) = -\frac{8}{9}\int_0^\infty y J_x^{\mathrm{PBE}}(s, y)\mathrm{d}y \tag{14}$$

with $s = |\nabla\rho|/2\pi k_F\rho$ the reduced gradient, k_F being the local Fermi vector, and $y = \mathrm{k}_F u$ the scaled interaction coordinate. For the analytic expression of J_x^{PBE}, the following parametrized form:

$$J_x^{\mathrm{PBE}}(s, y) = \left[-\frac{A}{y^2}\frac{1}{1 + (4/9)Ay^2} + \left(\frac{A}{y^2} + B + C[1 + s^2F(s)]y^2 + E[1 + s^2G(s)]y^4\right)\exp(-Dy^2)\right] \times \exp(-s^2H(s)y^2) \tag{15}$$

with parameters $A-E$ being constants and $F-H$ being functions of the reduced gradient, has been found by Ernzerhof et al. (see ref 28 for details). For the current purpose, the long-range enhancement factor is given by

$$F_x^{\mathrm{PBE,LRC}}(s) = -\frac{8}{9}\int_{R_c'}^\infty y J_x^{\mathrm{PBE}}(s, y)\mathrm{d}y \tag{16}$$

with $R_c' = R_c\mathrm{k}_F$. This integration can be carried out analytically (see Section A) yielding an expression for the long-range correction of the exchange energy.

The final form of the range-separated exchange energy reads now:

$$E_x = E_x^{\mathrm{HF,TC}}(R_c) + E_x^{\mathrm{PBE,LRC}}(R_c) \tag{17}$$

both parts depending on the cutoff radius, R_c. Using these results, one can define three different hybrid functionals:

$$\text{PBE0: } E_{\mathrm{xc}}^{\mathrm{PBE0}} = aE_x^{\mathrm{HF}} + (1 - a)E_x^{\mathrm{PBE}} + E_c^{\mathrm{PBE}} \tag{18}$$

$$\text{PBE0−TC: } E_{\mathrm{xc}}^{\mathrm{PBE0-TC}} = aE_x^{\mathrm{HF,TC}} + (1 - a)E_x^{\mathrm{PBE}} + E_c^{\mathrm{PBE}} \tag{19}$$

$$\text{PBE0−TC−LRC: } E_{\mathrm{xc}}^{\mathrm{PBE0-TC-LRC}} = aE_x^{\mathrm{HF,TC}} + aE_x^{\mathrm{PBE,LRC}} + (1 - a)E_x^{\mathrm{PBE}} + E_c^{\mathrm{PBE}} \tag{20}$$

PBE0 is, for $a = 0.25$, the standard PBE hybrid functional.[29−31] PBE0-TC denotes the original functional of PBE0 in which the standard HFX energy is replaced by the TC expression with cutoff radius R_c, and PBE0-TC-LRC is the PBE0-TC functional with the long-range correction (LRC) based on the PBE exchange hole. Of course, similar variants can be defined for other hybrid functionals. It is demonstrated in Section 3.2 that the use of a LRC allows for a very small R_c (≈ 2 Å) without negatively impacting the performance of the functional for typical thermochemical quantities. HFX with such a short-range can be evaluated very efficiently. Note that, in the limit of R_c going to zero, the PBE functional is recovered but based in part on the spherically averaged PBE exchange hole.

2.3. Efficient Calculation of Two-Electron Integrals for General $g(r)$. Two-electron four center integrals are commonly calculated analytically using recurrences.[32−34] CP2K employs the LIBINT[56] library for this. These algorithms start from the lowest angular momentum interaction, i.e., $(ss|ss)_g$, for a given interaction potential $g(r_{12})$ and then recursively calculate higher order contributions from that. In order to calculate integrals with a total angular momentum n, these routines have to be provided with $n + 1$ initial values as the starting vector. With the notation used by Ahlrichs,[34] this reads as

$$G_n(\rho, T) = \left(-\frac{\partial}{\partial T}\right)^n G_0(\rho, T) \tag{21}$$

$$G_0(\rho, T) = \frac{2\pi}{\rho^{3/2}\sqrt{T}} \int_0^\infty g\left(\frac{y}{\sqrt{\rho}}\right) y e^{-y^2-T} \sinh(2y\sqrt{T}) \mathrm{d}y \tag{22}$$

where T and ρ are parameters determined by the geometry and the involved Gaussian basis functions. For several commonly used operators, there exist efficient recursive formulas to calculate the higher order derivatives. In the case of the full range Coulomb potential, the whole procedure reduces to an evaluation of the Γ-function at various parameters T. For the TC potential one arrives at

$$G_0(\rho, T, R'_c) = \frac{\pi^{3/2}}{2\rho} \frac{2\mathrm{erf}(\sqrt{T}) + \mathrm{erf}(R'_c - \sqrt{T}) - \mathrm{erf}(R'_c + \sqrt{T})}{\sqrt{T}} \tag{23}$$

which depends on the parameter T and the cutoff radius $R'_c = R_c\sqrt{\rho}$. Unfortunately, there is no obvious recurrence to compute higher order derivatives, but (lengthy) explicit formulas are readily derived. Nevertheless, since the explicit dependence on ρ is trivial, it is sufficient to be able to evaluate the bivariate function (R'_c and T) and its derivatives, with respect to T to be able to evaluate the required four center integrals. An example of a higher order derivative is shown in Figure 1. Here, a largely automatic approach is presented that yields an accurate and efficient procedure to evaluate representations of these bivariate functions. This approach can be used with general operators $g(r)$ even if no explicit recurrences are known or if the numerical evaluation is troublesome. For example, the procedure has also been tested on the Yukawa potential for which Ten-no[22] skillfully derived a sequence of suitable expressions. Therefore, this technique might be useful for investigating density functionals that are based on a more flexible form of $g(r)$.

In a first step, computer code for the explicit calculation of the function and the required derivatives is generated by a computer algebra system. This can be either an explicit expression, as obtained for the TC operator, a symbolic Taylor series,[34] or any other convenient representation. Neither efficiency nor stability of the generated expression are a particular concern at this point. On a potentially large set of reference points, to be discussed below, this code is evaluated with arbitrary precision using a multi-precision floating point library (mpfr).[35,36] By doubling the number of digits employed in this evaluation until the result is accurate, a good numerical quality of the reference data is guaranteed. In order to evaluate accurately the higher derivatives of the TC operator, hundreds of digits are essential for the intermediate expressions. Finally, an automatic piece-wise bivariate interpolation of these reference points, using Chebyshev polynomials, is performed. This bivariate interpolation is constructed using the algorithm of Caliari et al.[37] In this scheme, the full two-dimensional parameter space has to be mapped first on the square $[-1, 1]^2$, which is the natural domain for the interpolation. The function must also be defined on the boundary of the domain. In this square, the Padua2D points of order n are a special set of optimal nodes used for the polynomial interpolation:

$$\xi = (\xi_1, \xi_2) = \left\{\gamma\left(\frac{k\pi}{n(n+1)}\right), \quad k = 0, ..., n(n+1)\right\} \tag{24}$$

with the generating curve:

$$\gamma(t) = (-\cos((n+1)t), -\cos(nt)), \qquad t \in [0, \pi] \tag{25}$$

The usage of these points guarantees an almost optimal convergence with increasing degree of the Chebyshev basis functions. The polynomial interpolation of a two-dimensional function $f(x_1, x_2)$ is then given by

$$f(x_1, x_2) \approx \sum_{k=0}^{n} \sum_{j=0}^{k} c_{j,k-j} \hat{T}_j(x_1) \hat{T}_{k-j}(x_2) - \frac{c_{n,0}}{2} \hat{T}_n(x_1) \hat{T}_0(x_2) \tag{26}$$

where the coefficients:

$$c_{j,k-j} = \sum_{\xi \in [1,1]^2} f(\xi) w_\xi \hat{T}(\xi_1) \hat{T}_{k-j}(\xi_2), \qquad 0 \le j \le k \le n \tag{27}$$

with weights w_ξ and Chebyshev polynomials $\hat{T}_m$ of order m can be computed once and for all and, thus, be stored in a table. Using the multi-precision enabled code, these coefficients are computed and stored in a standard 64-bit floating point representation. Function values of a bivariate function are then evaluated based on eq 26 and, thanks to the favorable properties of the Chebyshev expansion, will be accurate to nearly machine precision, provided the expansion is of sufficient order. This also holds for the G_n functions required for the TC operator.

However, since the target function typically shows different behavior in terms of smoothness and continuity at different argument ranges, it is not beneficial to perform a global interpolation, as this requires a high order and, thus, expensive interpolation. Instead, an adaptive scheme has been devised that, given a specified low order of the expansion, automatically bisects the full domain (e.g., using alternate directions) until the accuracy of the interpolation is accurate to a given threshold (e.g., 10^{-12} or machine precision). This procedure is facilitated by the fact that the Padua2D interpolation procedure provides an automatic estimate of the accuracy.[37] As the procedure bisects the domain, computer code is generated such that the proper interpolation

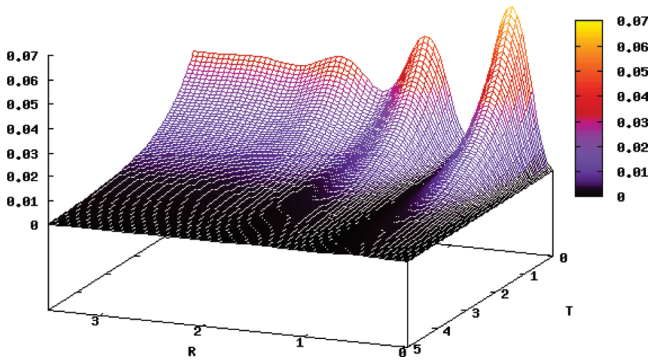

Figure 1. The figure shows $G_{14}(R'_c, T)$ as defined by eqs 21 and 23 for the TC operator.

coefficients can be found efficiently in a table of patch-wise interpolating functions. In this way, evaluations of the interpolation can be performed orders of magnitude more efficiently than with the global interpolation. For the case of the TC operator, an interpolation order of 13 has been employed. The down-side is, of course, that the interpolation is only piece-wise contiguous but nevertheless accurate to the chosen threshold everywhere. Note, that the interpolation is constructed for all derivatives simultaneously, i.e. eq 26, is never explicitely derived. In terms of efficiency, it can be concluded that calculating the starting vector $\mathbf{G}_n$ for the truncated potential is approximately twice as expensive as computing with an optimized implementation of the Γ-function, the starting vector for the full Coulomb potential. The code for evaluating $\mathbf{G}_n$ for the truncated potential is available, as is the code for constructing the adaptive interpolation.[38]

3. Assessment and Validation of the Method

3.1. Illustration on Gas- and Condensed-Phase Systems. In this section, the convergence behavior of the truncated operator for increasing cutoff radius R_c is investigated. As model systems, chains of poly-ethylene and poly-acetylene with a length of about 38 Å (30 carbon atoms) have been chosen. For both systems, self-consistent total energies have been calculated with the Hartree−Fock/pc-2[39−41] level of theory applying the standard Coulomb operator, which serves as a reference, and with the truncated operator for different cutoff radii in the range of 0.1−15 Å. In order to illustrate the effect of the long-range correction, the same calculations have been performed again, including the correction based on the PBE exchange hole. In addition, similar data for a two-dimensional hexagonal boron−nitride mesh in periodic boundary conditions are presented. The latter system consists of 128 atoms in total, has a dimension of 20.1 × 17.4 Å and was computed with a pc-1 basis set.[39−41] The reference value has been obtained from an exponential extrapolation of the last three data points.

All findings are summarized in Figure 2. In the case of the uncorrected TC operator, one observes that the total energy of all three systems decreases monotonically to the limiting value for increasing cutoff radius R_c. Furthermore, the logarithmic plot shows that all calculations converge approximately exponentially to the correct value. The faster convergence for poly-ethylene relative to poly-acetylene can directly be attributed to its larger band gap. The computed HF band gaps are 13.67, 7.34, and 13.95 eV for poly-ethylene, poly-acetylene, and the hexagonal boron−nitride mesh, respectively. The long-range correction improves upon the uncorrected total energies in the short-range (0−2.5 Å) but overestimates the correction to the total energy in the long-range part. It is not so surprising that the LRC does not capture the tail of the exchange hole very well, since the underlying model is essentially derived to capture the short-range behavior of the exchange hole. It appears that this model does not decay sufficiently fast. Very accurate Hartree−Fock energies are, thus, obtained more easily without correction.

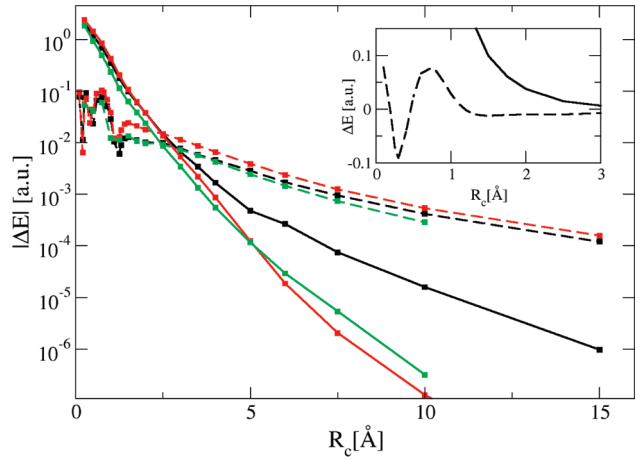

Figure 2. Shown are absolute errors in total energies with respect to the limiting case $R_c \rightarrow \infty$. Results for nonperiodic poly-ethylene and poly-acetylene are drawn in red and black, respectively, while results for periodic hexagonal boron−nitride are displayed in green. Solid and dotted lines represent data obtained without and with the long-range correction. All errors are scaled by the number of non-hydrogen atoms in each system. As shown in the inset for poly-acetylene, the correction over and under estimates the total energy at different ranges, which is the cause of the spikes in the logarithmic plot.

This analysis suggests that HFX calculations with a TC potential could serve as an interesting tool for investigating the behavior of the exchange hole at different ranges and could support the development of new density-based exchange hole models.

3.2. Barrier Heights and Reaction Energies for Gas-Phase Reactions. In order to analyze the accuracy of calculations based on the TC potential, the method has been benchmarked against a database established by Truhlar et al.[42] This database consists of 22 reactions involving 47 molecules in gas phase and provides geometries of reactants, products, and saddle points. This database has been selected because reaction energies are particularly sensitive to the precise treatment of exchange and because saddle point geometries usually involve somewhat delocalized electronic states. The dependence of the reaction energies and the barrier heights on the choice of R_c for both the PBE0-TC and PBE0-TC-LRC functionals has been investigated. In order to provide a reference, a comparison of these results to the established PBE,[5] PBE0,[29−31] HSE06,[7,8] and MCY3[21] functionals are presented. In addition, all benchmark runs have been performed twice, once with an all-electron representation and once applying pseudo-potentials. All-electron calculations employ the Gaussian and augmented plane waves (GAPW) method[43] and the MG3S basis,[44] while pseudo-potential calculations use the Gaussian and plane-waves (GPW) method,[45] PBE optimized pseudo-potentials,[46] and molecularly optimized TZV2P basis sets.[47] All results are summarized in Table 3. The first observation is that, as expected, the results of the standard PBE0 calculations are recovered as $R_c \rightarrow \infty$. Based on these results, the replacement of the standard HFX expression with its truncated counterpart seems to be possible without loss of accuracy, if $R_c > 6.0$ Å. As emphasized before, this is system dependent but appears

Table 3. The Table Shows Mean-Square Errors in kcal/mol of Classical Barrier Heights and Classical Reaction Energies with Respect to Experimental Values[a]

	GAPW		GPW	
	barriers	energies	barriers	energies
PBE	9.9	3.3	9.1	2.3
PBE0	4.6	1.7	4.3	2.0
HSE06	4.6	1.7	4.4	2.1
MCY3	2.9	1.7	3.0	1.3

R_c [Å]	TC	TC-LRC	TC	TC-LRC	TC	TC-LRC	TC	TC-LRC
∞	4.6	4.6	1.7	1.7	4.3	4.3	2.0	2.0
8.0	4.6	4.6	1.7	1.7	4.3	4.3	2.0	2.0
6.0	4.6	4.6	1.7	1.7	4.3	4.3	2.0	2.0
4.0	4.4	4.5	1.7	1.7	4.2	4.2	2.0	2.0
3.5	4.2	4.2	1.7	1.7	4.0	4.0	2.0	2.0
3.0	3.8	3.8	1.7	1.7	3.5	3.6	2.0	2.0
2.5	3.2	3.2	1.5	1.6	3.0	3.0	1.9	1.9
2.0	**2.7**	**2.6**	**1.4**	**1.4**	**2.5**	**2.5**	**2.0**	**1.9**
1.5	3.4	3.3	1.5	1.5	3.1	3.1	2.1	2.1
1.0	5.0	5.0	3.1	2.0	4.5	4.7	2.5	2.0
0.5	7.6	8.8	2.6	2.1	7.4	8.5	2.3	2.7

[a] The data is shown for standard functionals PBE, PBE0, HSE06, and MCY3 and for the TC PBE0-TC and long-range corrected PBE0-TC-LRC functionals. For the latter two functionals, truncation radii (R_c) ranging from 0.5 to 8.0 Å have been employed. Calculations have been performed using an all-electron approach (GAPW) with a MG3S basis and using pseudo-potentials (GPW) with a molecularly optimized TZV2P basis. Relative to experiment, the best results are obtained for $R_c = 2.0$ Å, shown in bold.

to hold for the (small) molecules in this test set. Interestingly, already for $R_c = 4.0$ Å, results obtained with either PBE0-TC and PBE0-TC-LRC are basically converged. If some small influence on the final results can be tolerated, a choice of $R_c = 4.0-6.0$ Å appears appropriate, which can bring noticeable savings in computer time for large systems. PBE0-TC and PBE0-TC-LRC appear only significantly different at short-range $R_c \leq 2.5$ Å.

For the very short-range calculations ($R_c = 0.5$ Å), where only the PBE0-TC-LRC functional is meaningful, the calculations yield, as expected, approximately PBE results. It can be observed that in the intermediate range, around $R_c = 2.0$, the best estimates are obtained for the reaction barriers, similar in quality to MCY3. This suggests that the use of very short-range exchange functionals, such as PBE0-TC-LRC at $R_c = 2.0$ Å is meaningful, and that even more accurate functionals that explicitly limit the action of exact exchange to such a short distance can be developed.

3.3. Parallel Performance. Given the computational cost of simulations including exact exchange, an efficient and scalable implementation is essential if exact exchange is to be a successful ingredient for simulations of large and complex systems. The initial implementation presented in ref 13 scaled to a few hundreds of cores for a condensed phase system containing 64 water molecules, described with a TZV2P basis for both oxygen and hydrogen (2560 basis functions). Combined with an in-core compression scheme and a multiple-time step approach, this was sufficient to compute 13 ps of MD trajectory. As shown in Figure 3, the new implementation, using the PBE0-TC-LRC($R_c = 2.0$) functional, allows the same system to scale up to a few

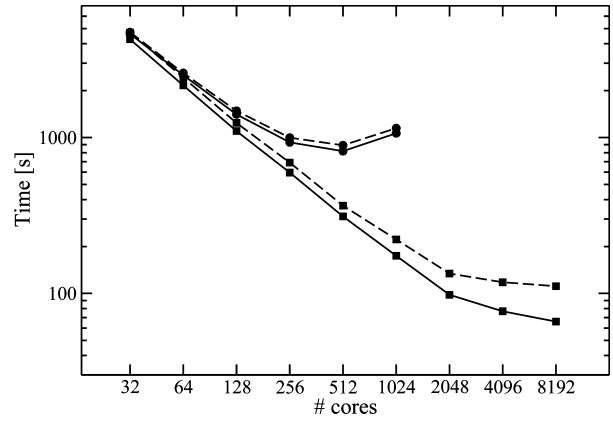

Figure 3. A comparison of the scaling of the current (squares) and previous (circles, ref 13) implementation of periodic HFX. The benchmark is 10 steps of ab initio molecular dynamics of 64 water molecules in PBC using a TZV2P basis and pseudo potentials. The solid lines represent the time spent in the HFX routines, and the dashed lines represent the total run time. Using 2 048 cores, successive Born−Oppenheimer MD steps take approximately 9 s. All timings were on a Cray XT5 with 8 cores per node.

thousands of cores, effectively allowing simulations to proceed 10 times faster. Currently, 10 ps of simulation can be obtained in two days, even without a multiple-time step scheme. As will be illustrated in Section 3.4, for systems that are computationally more demanding than 64 water molecules, scalability to 10′000s of cores can be reached effectively enabling CP2K[19] to obtain good performance on the largest supercomputers currently available.

The basic parallelization strategy has remained unchanged from the initial implementation, i.e., replicated density, and Kohn−Sham matrices are made available on all MPI processes. Based on a load-balancing step, the work of each process is decided in advance, and computation proceeds in a communication-free way until all local contributions to the Kohn−Sham matrix have been computed and until the matrix can be redistributed and summed. One key advantage of this approach is that full integral symmetry can be exploited. Furthermore, there are only communication steps in the beginning and end, and these can be performed efficiently in a ring topology. The disadvantage of this approach is that neither the communication nor the memory decreases as the number of processes increases. The memory bottleneck limits the size of the systems that can be studied, while the communication bottleneck ultimately limits scalability, provided the load balance can be maintained throughout. However, the current implementation reduces the impact of the matrix replication by employing a mixed MPI/openMP scheme, where density and Kohn−Sham matrix are shared between the threads (one per core) on a node. In this way, the communication needed for the replication is reduced, and, depending on the available RAM, much larger systems (3×10^4 basis functions and more for 16 Gb/node) can fit in memory. A further benefit of the MPI/openMP scheme is that load balancing between threads can easily be performed. Such a dynamic load balancing is helpful for inhomogeneous systems that are difficult to load balance before the calculations start. Nevertheless, the importance of a good initial

Table 4. Results Obtained with the Truncated Coulomb Operator and a Large and Flexible Basis for Unit Cells That Are a Multiple of the Basic Cubic Unit Cell (4.084 Å)[a]

	R_c [Å]	E(HF)[au]	H[au]	Li[au]	ε_{HF}^{coh} [au]
2 × 2 × 2	4.0	−32.244609	−0.499957	−7.428493	−0.132702
3 × 3 × 3	6.0	−32.256844	−0.499974	−7.432137	−0.132100
4 × 4 × 4	8.0	−32.258022	−0.499974	−7.432582	−0.131949
5 × 5 × 5	10.0	−32.258179	N/A	N/A	N/A

[a] The columns show the size of the unit cell, the range of the TC operator (R_c), the Hartree−Fock energy per unit cell, the H atom energy, the Li atom energy, and the cohesive energy, respectively (ε_{HF}^{coh}).

distribution of work cannot be underestimated, and a carefully constructed load-balancing algorithm is essential. The full description of this part of the algorithm is beyond the scope of the current paper. The basic ingredient is a binning procedure that collects batches of four center integrals of approximately equal estimated computational cost. These bins, typically 64 per core, are the basic unit of work and are distributed such that the computational load is balanced.

3.4. The Cohesive Energy of LiH at Hartree−Fock Basis Set Limit. Recent HF and post-HF results on crystalline LiH[48−57] have received much interest in the solid-state community. The availability of accurate reference numbers has made this system a challenging benchmark to judge the accuracy of various theoretical methods applied to condensed-phase systems. This work contributes to this ongoing research by computing the HF cohesive energy of LiH near the basis set limit. These results have been published in part in ref 51, where a comparison of the total energy of the LiH crystal obtained directly using the truncated method with results by Scuseria and co-workers based on extrapolation of screened exchange has been presented. Here, these results are summarized, and more details of these calculations are presented.

In a first step, an optimized basis set for an accurate HF calculation on bulk LiH, similar in composition to the polarization consistent (pc-3) basis sets derived by Jensen,[39−41] has been constructed. The composition of this basis set is 8s3p2d1f/6s3p2d1f and 13s6p2d1f/11s5p2d1f for hydrogen and lithium (see ref 51 for details). The accuracy of the optimized basis has been estimated to be within 0.001 au of the basis set limit for the total energy, while the basis set error on the cohesive energy is likely smaller than 0.1%. All calculations, summarized in Table 4, have been performed on the experimental cubic unit cell with linear dimension $L = 4.084$ Å, which contains 4 Li and 4 H atoms, using truncated HF without the long-range correction. Total energies have been computed for systems of increasing system size by explicitely repeating this unit cell periodically in three dimensions. The largest system employed, a 5 × 5 × 5 repetition, consists of exactly 1 000 atoms and uses 37 500 Gaussian basis functions. With increasing system size, the range of the TC operator has been increased as well. The results have been found to converge exponentially with system size, and an accurate estimate for the total energy per unit cell of approximately −32.258179 au could be obtained directly from a calculation of the largest system. This number is in excellent agreement with the Padé-extrapolated SR-HFX results of ref 51 −32.258171 au. By calculating the HF energy of the H and Li atoms in periodic boundary conditions and retaining the basis functions of all other (ghost) atoms in the unit cell, a consistent number for the cohesive energy could be obtained. However, due to the fact that unrestricted calculations are needed for the atoms, these calculations are more demanding (memory-wise) than the bulk and are, therefore, only performed for the 4 × 4 × 4 repetition of the basis cell. The 4 × 4 × 4 crystal required 11 terabytes of memory for the integral storage. The best estimate of the cohesive energy obtained in this way is −131.949 mE_h. This result is derived in an extrapolation-free way and based on just three calculations (bulk LiH and the atoms Li and H). It is in very good agreement with the best estimate reported by Gillan et al.,[48] −131.95 mE_h. In order to investigate quantitatively the convergence of the energies with respect to R_c, systematic calculations of the HFX energies for the 5 × 5 × 5 unit cell, using a smaller basis set (adjusted pc-2 basis 4s2p1d/4s2p1d and 9s3p1d/9s3p1d for H and Li, respectively, 19 000 basis functions in total) have been performed. These results are presented in Table 5 and show that the cohesive energy is obtained with milli-Hartree accuracy for $R_c = 6$ Å and micro-Hartree accuracy for $R_c = 10$ Å.

Table 5. Hartree−Fock results Obtained with the Truncated Coulomb Operator for Various Values of R_c without Long-Range Correction[a]

R_c [Å]	E(HF)[au]	H[au]	Li[au]	ε_{HF}^{coh} [au]
3	−32.231006	−0.498769	−7.405766	−0.153216
4	−32.242905	−0.499298	−7.423518	−0.137911
5	−32.246980	−0.499325	−7.429613	−0.132807
6	−32.247893	−0.499326	−7.431395	−0.131252
7	−32.248177	−0.499326	−7.431845	−0.130873
8	−32.248275	−0.499326	−7.431944	−0.130798
9	−32.248308	−0.499326	−7.431964	−0.130787
10	−32.248321	−0.499326	−7.431967	−0.130787

[a] The 5 × 5×5 repetition of the basic cubic unit cell (4.084 Å) has been employed, together with a smaller basis set. The columns show the range of the TC operator (R_c), the Hartree−Fock energy per unit cell, the H atom energy, the Li atom energy, and the cohesive energy, respectively (ε_{HF}^{coh}).

This system has also been used to measure the parallel efficiency of the implementation. Using the 3 × 3 × 3 repetition of the basic unit cell, consisting of 216 atoms and 8 100 basis functions, calculations, taking advantage of the hybrid MPI/openMP approach discussed above, have been performed. The results for this setup, summarized in Figure 4, show that this approach scales beyond 32 768 cores. The scaling is superlinear up to approximately 2 048 cores because the increasing amount of memory (2Gb/core) is used to store four center integrals, and successive SCF steps benefit from the in-core storage. The total amount of storage used for integrals exceeds 3 terabytes in this case. For the runs on more than 16 384 cores, the impact of the com-

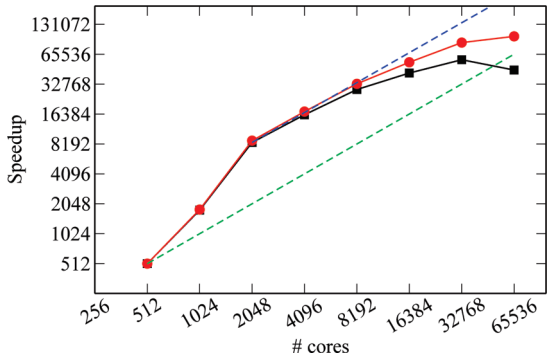

Figure 4. Shown is the speedup obtained from a computation of the 3 × 3 × 3 repetition of the basic unit cell of LiH (8 100 basis functions). Black and red curves depict the observed speedups for the full calculation and for the Hartree−Fock part, respectively. Dotted lines correspond to theoretical speedups, assuming either an infinite amount of memory per node (blue) or the actually 16 Gb/node (green). All calculations have been performed using 8 threads per MPI process on a 8 core node (CRAY XT5).

munication becomes significant and ultimately limits scalability. For this system, the load balance remains excellent and the local construction of the Fock matrix itself scales perfectly even at 65 536 cores.

3.5. The Electronic Structure of Rubredoxin. In order to demonstrate the ability of the TC method to compute large, inhomogeneous condensed phase systems with high quality basis sets, the electronic structure of a fully solvated iron−sulfur protein, rubredoxin, in periodic boundary conditions with a polarized triple-ζ valence basis set[52] for all atoms, including hydrogen, has been computed. In this setup, the system is described with 31 247 basis functions, containing 2 825 atoms, and the unit cell has edges 31.136 × 28.095 × 30.502 Å^3. Due to the iron−sulfur active site, the multiplicity of the system is 6. The same system has been employed in earlier work with semilocal functionals to demonstrate the ability to compute ab initio free energy differences[53] and total energies near the basis set limit[47] for systems containing nearly 3 000 atoms. A single-point wave function optimization takes less than two hours, with about two-thirds of the time spent in the HFX routines using 8 196 cores of a CRAY XT5. The storage needed for the integrals is approximately 2.5 terabytes, using a threshold of 10^{-8} for Schwarz screening and an in-core compression scheme described in ref 13. With this calculation, the difference in spin density distribution for the active site between a hybrid functional (B3LYP[2,4,54,55]) with the TC operator (R_c = 6.0 Å) and a semilocal functional (BLYP[3,4]) has been investigated. The result of the calculation is illustrated in Figure 5 where the difference in spin density between the GGA and the hybrid calculation is shown. Not unexpectedly, a more localized spin density is found with the hybrid functionals.

4. Conclusions

A new approach for Hartree−Fock calculations at the Γ-point using Gaussian basis functions has been presented. This approach is based on the TC operator and is demonstrated to be robust. With increasing truncation radius, results converge exponentially to the limiting Hartree−Fock values. Furthermore, a density functional based long-range correction to the TC operator has been derived. With this correction, a very short-range exchange (R_c = 2.0 Å) yields excellent results for reaction energies and for barrier heights. The finite range of the operator allows for efficient screening and can be exploited in a linear-scaling implementation of exchange. The current implementation is massively parallel and allows for calculations on systems containing thousands of atoms and ten thousands of basis functions. These developments will enable simulations based on hybrid functionals that probe the rich chemistry and the physics of large and complex condensed-phase systems.

5. Appendices

A. Long-Range Correction. In this section, analytical expressions for the long-range part of the PBE exchange hole enhancement factor are presented in closed form for any given cutoff radius R_c. Indeed, based on $J_x^{\mathrm{PBE}}(s, y)$ as defined by eq 15 (see ref 28 for details, including definition of the quantities A−H), one finds that:

$$F_x^{\mathrm{PBE,LRC}}(s) = -\frac{8}{9}\int_{R_c'}^{\infty} y J_x^{\mathrm{PBE}}(s,y)\mathrm{d}y = -\frac{8}{9}(I_1 - I_2 + I_3 + I_4) \quad (28)$$

where:

$$I_1 = -\frac{A}{2}\exp\left(\frac{9}{4}\frac{s^2H}{A}\right)\mathrm{Ei}\left(-\frac{9}{4}\frac{s^2H}{A} - s^2HR_c'^2\right) \quad (29)$$

$$I_2 = -\frac{A}{2}\mathrm{Ei}(-s^2HR_c'^2) \quad (30)$$

$$I_3 = -\frac{A}{2}\mathrm{Ei}(-(D + s^2H)R_c'^2) \quad (31)$$

$$I_4 = \alpha(\alpha_0 + \alpha_2R_c'^2 + \alpha_4R_c'^4)\exp(-R_c'^2(D + Hs^2) \quad (32)$$

with

$$\alpha = \frac{1}{2}\frac{1}{(D + s^2H)^3} \quad (33)$$

$$\alpha_0 = 2E + DC + D^2B + s^2(HC + 2DHB + 2EG + DCF) + s^4(H^2B + HCF) \quad (34)$$

$$\alpha_2 = D^2C + 2DE + s^2(2EH + 2DEG + 2DHC + D^2CF) + s^4(2EGH + 2DHCF + CH^2) + s^6CFH^2 \quad (35)$$

$$\alpha_4 = D^2E + s^2(D^2EG + 2DHE) + s^4(2DHEG + EH^2) + s^6EGH^2 \quad (36)$$

and:

$$R_c' = R_c\mathrm{k}_F \quad (37)$$

$\mathbf{k}_F$ denoting the local Fermi vector. Ei(x) is the exponential integral and defined as

$$\mathrm{Ei}(x) = \int_{-\infty}^{x} \frac{e^t}{t} \mathrm{d}t \tag{38}$$

B. Stability Criterion. In this section, the effect of thresholding and the MIC on the stability of the SCF is analyzed. Starting from the exchange energy for a system containing N basis functions:

$$E_x^{\mathrm{HF}} = -\frac{1}{2} \sum_{\mu\nu\lambda\sigma} P^{\mu\sigma} P^{\nu\lambda} (\mu\nu|\lambda\sigma)_g \tag{39}$$

which can be rewritten in terms of matrix−vector products as the quadratic form

$$E_x^{\mathrm{HF}} = \mathbf{P}^T \mathbf{v}_{\mathrm{exact}} \mathbf{P} \tag{40}$$

where $\mathbf{v}_{\mathrm{exact}}$ is a $N^2 \times N^2$ matrix containing all four center integrals, and $\mathbf{P}$ is a vector of size N^2 with the density matrix elements. If screening is applied to the four center integrals using a given threshold ε, the above equation can be written as

$$E_x^{\mathrm{HF}} = \mathbf{P}^T \mathbf{v}_{\mathrm{screened}} \mathbf{P} + \mathbf{P}^T \mathbf{v}_\varepsilon \mathbf{P} \tag{41}$$

where $\mathbf{v}_{\mathrm{screened}}$ collects all integrals that pass the screening, i.e., contributions that are larger than the threshold, and $\mathbf{v}_\varepsilon$ is a matrix of error terms of order $\mathcal{O}(\varepsilon)$ that are ignored throughout the calculation. For a reliable and stable optimization procedure, the maximum error introduced by ignoring $\mathbf{P}^T \mathbf{v}_\varepsilon \mathbf{P}$ should be small.

In order to get an estimate for the maximum magnitude of the error, it is sufficient to obtain an estimate of the maximum eigenvalue of the $\mathbf{P}$ matrix because

$$\mathbf{P}^T \mathbf{v}_\varepsilon \mathbf{P} \leq \lambda_{\max}^2(\mathbf{P})\, \mathcal{O}(\varepsilon) \tag{42}$$

The above formula can be derived under the assumption that the largest eigenvalue of $\mathbf{v}_\varepsilon$ is $\mathcal{O}(\varepsilon)$. In the worst case, this eigenvalue could be $N^2\varepsilon$ but is usually smaller ($\sim N\varepsilon$).

Since $\mathbf{C}^{\mathrm{T}}\mathbf{S}\mathbf{C} = 1$ with $\mathbf{C}$ being the matrix of the molecular orbitals, and $\mathbf{S}$ the overlap matrix of the basis functions, the following upper bound for the norm of $\mathbf{C}$ can be obtained

$$||\mathbf{C}|| \leq \frac{1}{\sqrt{\lambda_{\min}(\mathbf{S})}} \tag{43}$$

Writing the density matrix $\mathbf{P}$ in terms of molecular orbitals, $\boldsymbol{P} = \mathbf{C}\mathbf{C}^{\mathrm{T}}$, one finds that:

$$\lambda_{\max}^2(\mathbf{P}) \leq \frac{1}{\lambda_{\min}^2(\mathbf{S})} \tag{44}$$

Finally, the above expression can be related to the condition number of the overlap matrix:

$$\kappa(\mathbf{S}) = \frac{\lambda_{\max}(\mathbf{S})}{\lambda_{\min}(\mathbf{S})} \approx \frac{1}{\lambda_{\min}(\mathbf{S})} \tag{45}$$

where the largest eigenvalue of $\mathbf{S}$ is assumed to be of order one. Based on these estimates, one can conclude that the SCF calculations will be stable as long as

$$\varepsilon \leq \mathcal{O}\left(\frac{1}{\kappa^2(\mathbf{S})}\right) \tag{46}$$

This stability estimate is usually too conservative but it does represent a worst-case scenario. On the other hand, as long as the SCF is stable, it is usually observed that $\lambda_{\max}(\mathbf{P}) \approx \mathcal{O}(1)$, which confirms that the error due to screening is typically ε per electron.

Finally, an analysis of the instability observed with the MIC algorithm is presented. Essentially, the MIC can be interpreted as a calculation with a TC potential using $R_c = L/2$ but with two sources of error in the computed four center integrals. The first source of error is due to the fact that only one term in the sum over $\mathbf{b}$ is retained, while the second source of error is due to the fact that these integrals are computed with the $1/r$ operator. These errors add an additional term $\mathbf{v}_{\mathrm{MIC}}$ to the expression:

$$E_x^{\mathrm{HF}} = \mathbf{P}^T \mathbf{v}_{\mathrm{screening}} \mathbf{P} + \mathbf{P}^T \mathbf{v}_\varepsilon \mathbf{P} + \mathbf{P}^T \mathbf{v}_{\mathrm{MIC}} \mathbf{P} \tag{47}$$

which can not be controlled by the threshold ε. As before, the error related to $\mathbf{P}^T \mathbf{v}_{\mathrm{MIC}} \mathbf{P}$ might grow quickly as the condition number of the basis set becomes worse, explaining

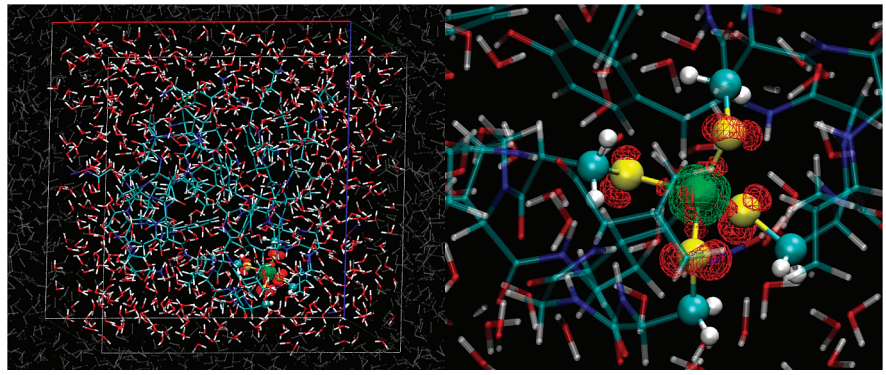

Figure 5. The left panel shows the unit cell of the solvated protein rubredoxin, while the right panel focuses on its iron−sulfur active site. The contour shows the difference in spin density distribution between calculations performed with BLYP and B3LYP with the TC operator. Red indicates an excess in spin density with the local functional, while green indicates an excess with the hybrid functional. Clearly, the use of a hybrid functional favors localization of the spin density.

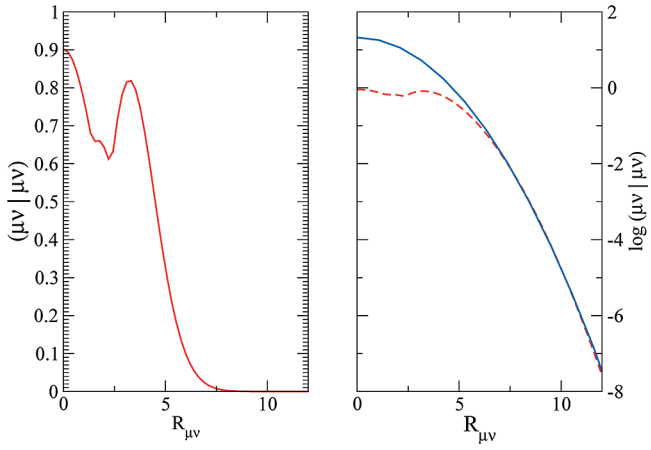

Figure 6. Shown are plots for $(\mu\nu|\mu\nu)$ as a function of the interatomic distance $R_{\mu\nu}$ for a lithium p-function and a hydrogen d-function. The left panel shows the calculated values and the right panel shows the logarithm of this data (dotted line) together with the fitting function (blue).

the stability of the algorithm with small and well-conditioned basis sets and the instability with large and flexible basis sets.

C. Efficient Near- and Far-Field Screening. Determining in advance which four center integrals are smaller than a given threshold and can, thus, be ignored in the calculation is important in an implementation of HFX that targets large systems. Indeed, screening reduces the number of integrals that need to be computed from $\mathcal{O}(N^4)$ to $\mathcal{O}(N)$. Two kinds of screening are commonly employed for the four center integrals, namely near- and far-field screening. Near-field screening[14] relies on the Schwarz-inequality and reduces the number of terms to $\mathcal{O}(N^2)$ also for calculations employing the $1/r$ operator, far-field screening only becomes really efficient[15] for operators $g(r)$ that decay faster than $1/r$ and reduces the number of required four center integrals to $\mathcal{O}(N)$. For systems with decaying density matrix (i.e., systems with an electronic gap), combining near-field screening with screening on the density matrix elements[16] also reduces the effort to $\mathcal{O}(N)$. A brute-force implementation of the screening, as implemented in CP2K,[19] is $\mathcal{O}(N^2)$. It is, therefore, important to reduce the prefactor of this term as much as possible and to have an efficient screening algorithm. An approach which is sufficiently efficient to deal with systems containing thousands of atoms without significant screening overhead is presented below.

For the near-field screening one can rely on the Cauchy−Schwarz inequality,

$$|(\mu\nu^{\mathbf{a}}|\lambda^{\mathbf{b}}\sigma^{\mathbf{b+c}})| \leq |(\mu\nu^{\mathbf{a}}|(\mu\nu^{\mathbf{a}})|^{1/2} \times |(\lambda\sigma^{\mathbf{c}}|\lambda\sigma^{\mathbf{c}})|^{1/2} \quad (48)$$

which only requires two center integrals. However, instead of storing or computing these two center integrals, it is very efficient to instead parametrize screening functions that are an upper bound to these integrals. These screening functions only depend parametrically on the interatomic distance $R_{\mu\nu}$ but are different for each type of Gaussian basis function (atom kind, shell, sets). These fits can be easily performed once one observes (see Figure 6) that the logarithm of the integral is similar to a quadratic function at larger distance:

$$\log((\mu\nu|\mu\nu)(R_{\mu\nu})) \approx a_2 R_{\mu\nu}^2 + a_0 \quad (49)$$

This choice leads to the useful properties that the estimate decays monotonically with increasing distance and that the expression only requires the square distance between the centers. The coefficients a_0 and a_2 are calculated once and for all at the beginning of a calculation, minimizing an asymmetric penalty function:

$$\sum_i k(\Delta_i)\Delta_i^2 \quad (50)$$

over a grid of suitably chosen values $R_{\mu\nu}^i$, with $\Delta_i = \log((\mu\nu|\mu\nu)(R_{\mu\nu})) - (a_2 R_{\mu\nu}^2 + a_0)$, and $k(\Delta_i) = 1$, if $\Delta_i < 0$ and $k(\Delta_i) = 1 \times 10^4$ otherwise. This choice of k guarantees that $a_2 R_{\mu\nu}^2 + a_0$ will be approximately an upper bound and not merely a least-squares fit. Clearly, once the coefficients are determined, obtaining a Schwarz estimate of the integral is particularly fast.

The far-field screening is currently based on a rather crude estimate, which only flags if the integral will be smaller than a given threshold. For the TC operator this estimate can be obtained easily. It is based on the radii of the product densities of $R_{\mu\nu}^{\rho}$ for $\mu\nu^{\mathbf{a}}$ and $R_{\lambda\sigma}^{\rho}$ for $\lambda^{\mathbf{b}}\sigma^{\mathbf{b+c}}$ and cycles as soon as $R_{\mu\nu}^{\rho} + R_{\lambda\sigma}^{\rho} + R_c < |\mathbf{P} - \mathbf{Q}|$, where $\mathbf{P}$ and $\mathbf{Q}$ are the centers of the product densities. The radii $R_{\mu\nu}^{\rho}$ and $R_{\lambda\sigma}^{\rho}$ are similarly obtained from a two-parameter fit to precomputed values.

Acknowledgment. J.V. acknowledges interesting discussions with J. Spencer and A. Alavi. The authors acknowledge E. Valeev for making LIBINT available under the Gnu public license. A fruitful collaboration with John Levesque (Cray Inc.) is also acknowledged. His extensive testing on the Cray XT5 (Jaguar) at the Oak Ridge National Laboratory (ORNL) enabled the massively parallel implementation of the Hartree−Fock code in CP2K. Additional computer resources have been provided by the Swiss National Supercomputing Center (CSCS) and, as part of the PRACE project, by the Finnish IT Center for Science (CSC). The PRACE project receives funding from the EU's Seventh Framework Programme (FP7/2007-2013) under grant agreement no. RI-211528.

References

(1) Dirac, P. A. M. *Math. Proc. Cambridge Philos. Soc.* **1930**, *26*, 376–385.

(2) Vosko, S. H.; Wilk, L.; Nusair, M. *Can. J. Phys.* **1980**, *58*, 1200–1211.

(3) Becke, A. D. *Phys. Rev. A: At., Mol., Opt. Phys.* **1988**, *38*, 3098.

(4) Lee, C. T.; Yang, W. T.; Parr, R. G. *Phys. Rev. B: Condens. Matter* **1988**, *37*, 785–789.

(5) Perdew, J. P.; Burke, K.; Ernzerhof, M. *Phys. Rev. Lett.* **1996**, *77*, 3865–3868.

(6) Tao, J. M.; Perdew, J. P.; Staroverov, V. N.; Scuseria, G. E. *Phys. Rev. Lett.* **2003**, *91*, 146401.

(7) Heyd, J.; Scuseria, G. E.; Ernzerhof, M. *J. Chem. Phys.* **2003**, *118*, 8207–8215.

(8) Heyd, J.; Scuseria, G. E.; Ernzerhof, M. *J. Chem. Phys.* **2006**, *124*, 219906 Erratum.

(9) Zhao, Y.; Truhlar, D. G. *Theor. Chem. Acc.* **2008**, *120*, 215.

(10) Zhao, Y.; Truhlar, D. G. *J. Chem. Phys.* **2006**, *125*, 194101.

(11) Zhao, Y.; Truhlar, D. G. *J. Phys. Chem. A* **2006**, *110*, 13126.

(12) Zhao, Y.; Truhlar, D. G. *Acc. Chem. Res.* **2008**, *41*, 157.

(13) Guidon, M.; Schiffmann, F.; Hutter, J.; VandeVondele, J. *J. Chem. Phys.* **2008**, *128*, 214104.

(14) Strout, D. L.; Scuseria, G. E. *J. Chem. Phys.* **1995**, *102*, 8448–8452.

(15) Izmaylov, A. F.; Scuseria, G. E.; Frisch, M. J. *J. Chem. Phys.* **2006**, *125*, 104103.

(16) Ochsenfeld, C.; White, C. A.; Head-Gordon, M. *J. Chem. Phys.* **1998**, *109*, 1663–1669.

(17) Tymczak, C. J.; Weber, V. T.; Schwegler, E.; Challacombe, M. *J. Chem. Phys.* **2005**, *122*, 124105.

(18) Spencer, J.; Alavi, A. *Phys. Rev. B: Condens. Matter* **2008**, *77*, 193110.

(19) *CP2K*, the CP2K developers group, is freely available from http://cp2k.berlios.de/ (2009).

(20) VandeVondele, J.; Krack, M.; Mohamed, F.; Parrinello, M.; Chassaing, T.; Hutter, J. *Comput. Phys. Commun.* **2005**, *167*, 103.

(21) Cohen, A. J.; Mori-Sánchez, P.; Yang, W. *J. Chem. Phys.* **2007**, *126*, 191109.

(22) Ten-no, S. *J. Chem. Phys.* **2007**, *126*, 014108.

(23) Gygi, F.; Baldereschi, A. *Phys. Rev. B: Condens. Matter* **1986**, *34*, 4405.

(24) Pisani, C.; Dovesi, R. *Int. J. Quantum Chem.* **1980**, *17*, 501–516.

(25) Wenzien, B.; Cappellini, G.; Bechstedt, F. *Phys. Rev. B: Condens. Matter* **1995**, *51*, 14701.

(26) Sorouri, A.; Foulkes, W. M. C.; Hine, N. D. M. *J. Chem. Phys.* **2006**, *124*, 064105.

(27) Carrier, P.; Rohra, S.; Görling, A. *Phys. Rev. B: Condens. Matter* **2007**, *75*, 205126.

(28) Ernzerhof, M.; Perdew, J. P. *J. Chem. Phys.* **1998**, *109*, 3313–3320.

(29) Perdew, J. P.; Ernzerhof, M.; Burke, K. *J. Chem. Phys.* **1996**, *105*, 9982–9985.

(30) Perdew, J. P.; Ernzerhof, M.; Burke, K. *Int. J. Quantum Chem.* **1997**, *64*, 285–295.

(31) Ernzerhof, M.; Scuseria, G. E. *J. Chem. Phys.* **1999**, *110*, 5029–5036.

(32) Obara, S.; Saika, A. *J. Chem. Phys.* **1986**, *84*, 3963–3974.

(33) Helgaker, T.; Jørgensen, P.; Olsen, J. *Molecular Electronic Structure Theory*; John Wiley & Sons: Chichester, U.K., 2000.

(34) Ahlrichs, R. *Phys. Chem. Chem. Phys.* **2006**, *8*, 3072–3077.

(35) Fousse, L.; Hanrot, G.; Lefèvre, V.; Pélissier, P.; Zimmermann, P. *ACM Trans. Math. Softw.* **2007**, *33*, 13.

(36) *The MPFR Library*, http://www.mpfr.org (2009). For additional reference information see ref 35.

(37) Marchi, M. C. S.; Vianello, M. *ACM Trans. Math. Softw.* **2008**, *35*, 1–11.

(38) *Fun2D*, the CP2K developers group, is freely available from http://cvs.berlios.de/cgi-bin/viewvc.cgi/cp2k/cp2k/tools/Fun2D/ (2009).

(39) Jensen, F. *J. Chem. Phys.* **2001**, *115*, 9113.

(40) Jensen, F. *J. Chem. Phys.* **2002**, *116*, 7372.

(41) Jensen, F. *J. Phys. Chem. A* **2007**, *111*, 11198–11204.

(42) Lynch, B. J.; Truhlar, D. G. *J. Phys. Chem. A* **2001**, *105*, 29362936.

(43) Krack, M.; Parrinello, M. *Phys. Chem. Chem. Phys.* **2000**, *2*, 2105–2112.

(44) Lynch, B. J.; Zhao, Y.; Truhlar, D. G. *J. Phys. Chem. A* **2003**, *107*, 1384.

(45) Lippert, G.; Hutter, J.; Parrinello, M. *Theor. Chem. Acc.* **1999**, *103*, 124.

(46) Krack, M. *Theor. Chem. Acc.* **2005**, *114*, 145–152.

(47) VandeVondele, J.; Hutter, J. *J. Chem. Phys.* **2007**, *127*, 114105.

(48) Gillan, M. J.; Alfe, D.; Gironcoli, S.; Manby, F. R. *J. Comput. Chem.* **2008**, *29*, 2098.

(49) Manby, F. R.; Alfe, D.; Gillan, M. J. *Phys. Chem. Chem. Phys.* **2006**, *8*, 5178.

(50) Marsman, M.; Grüneis, A.; Paier, J.; Kresse, G. *J. Chem. Phys.* **2009**, *130*, 184103.

(51) Paier, J.; Diaconu, C. V.; Scuseria, G. E.; Guidon, M.; VandeVondele, J.; Hutter, J. submitted.

(52) Schäfer, A.; Huber, C.; Ahlrichs, R. *J. Chem. Phys.* **1994**, *100*, 5829.

(53) Sulpizi, M.; Raugei, S.; VandeVondele, J.; Carloni, P.; Sprik, M. *J. Phys. Chem. B* **2007**, *111*, 3669.

(54) Becke, A. D. *J. Chem. Phys.* **1993**, *98*, 5648.

(55) Stephens, P. J.; Devlin, F. J.; Chabalowski, C. F.; Frisch, M. J. *J. Phys. Chem.* **1994**, *98*, 11623–11627.

(56) Valeev, E., Fermann, J. T. http://www.chem.vt.edu/chem-dept/valeev/software/libint/libint.html, 2009.

(57) Nolan, S. J.; Gillan, M. J.; Alfè, D.; Allan, N. L.; Manby, F. R. *Phys. Rev. B* **2009**, *80*, 165109.

CT900494G